



The Moho beneath western Tibet: Shear zones and eclogitization in the lower crust



Zhongjie Zhang^{a,1}, Yanghua Wang^b, Gregory A. Houseman^{c,*}, Tao Xu^a, Zhenbo Wu^a, Xiaohui Yuan^d, Yun Chen^a, Xiaobo Tian^a, Zhiming Bai^a, Jiwen Teng^a

^a Institute of Geology and Geophysics, Chinese Academy of Sciences, Beijing, 100029, China

^b Department of Earth Science and Engineering, Imperial College London, SW7 2AZ, UK

^c School of Earth and Environment, University of Leeds, LS2 9JT, UK

^d GFZ German Research Centre for Geosciences, Telegrafenberg, 14473 Potsdam, Germany

ARTICLE INFO

Article history:

Received 11 July 2014

Received in revised form 10 October 2014

Accepted 13 October 2014

Available online xxxx

Editor: A. Yin

Keywords:

Tibetan Plateau
Moho segmentation
receiver functions
crustal thickness
eclogitization
shear zones

ABSTRACT

The Tibetan Plateau is formed by continuing convergence between Indian and Asian plates since ~50 Ma, involving more than 1400 km of crustal shortening. New seismic data from western Tibet (the TW-80 experiment at 80°E) reveal segmentation of lower crustal structure by the major sutures, contradicting the idea of a mobile lower crust that flows laterally in response to stress variations. Significant changes in crustal structure and Moho depth occur at the mapped major tectonic boundaries, suggesting that zones of localized shear on sub-vertical planes extend through the crust and into the upper mantle. Converted waves originating at the Moho and at a shallower discontinuity are interpreted to define a partially eclogitized layer that extends 200 km north of the Indus–Yarlung Suture Zone, beneath the entire Lhasa block at depths of between 50 and 70 km. This layer is thinner and shallower to the north of the Shiquanhe Fault which separates the northern Lhasa block from the southern part, and the degree of eclogitization is interpreted to increase northward. The segmentation of the Tibetan crust is compatible with a shortening deformation rather than shear on horizontal planes. Unless the Indian-plate mantle lithosphere plunges steeply into the mantle beneath the Indus–Yarlung suture, leaving Indian-plate crust accreted to the southern margin of Tibet, then it too must have experienced a similar shortening deformation.

© 2014 Elsevier B.V. All rights reserved.

1. Introduction

Two basic mechanisms have been proposed to explain the high elevation of the Tibetan Plateau: crustal shortening and thickening (Allegre et al., 1984; England and Houseman, 1986), or underthrusting of Indian mantle lithosphere (Ni and Barazangi, 1984; Tilmann et al., 2003; Kumar et al., 2006; Rai et al., 2006; Li et al., 2008). Other processes that may have influenced the evolution of the Tibetan lithosphere and its plateau include lithospheric detachment (Kosarev et al., 1999) or convective thinning (Houseman et al., 1981), underplating (Nábělek et al., 2009), subduction of the Asian lithosphere (Kind et al., 2002), channel flow (Beaumont et al., 2001; Royden et al., 2008) and escape tectonics (Tapponnier et al., 1982; Replumaz and Tapponnier, 2003). These geodynamic processes are interpreted from structural mapping (Yin and Har-

ison, 2000) and from seismic profiling studies using both controlled source and teleseismic signals, with observations mainly from eastern and central Tibet (e.g., Hirn et al., 1984; Owens and Zandt, 1997; Schulte-Pelkum et al., 2005; Zhao et al., 2010; Mechie and Kind, 2013). Body and surface wave tomography have also provided important constraints on upper mantle structure (Tilmann et al., 2003; Priestley et al., 2006; Ren and Shen, 2008; Li et al., 2008; Replumaz et al., 2012; Liang et al., 2012; Razi et al., 2014).

Contrasting interpretations of how far the Indian plate extends underneath the plateau (Owens and Zandt, 1997; Kosarev et al., 1999; Nábělek et al., 2009; Kind and Yuan, 2010) and whether the lower crust of Tibet has been displaced by channel flow (Beaumont et al., 2001; Royden et al., 2008; Rey et al., 2010) have focused debate on these questions. Using new data from a NS seismic profile across western Tibet, we show that: (1) the entire thickness of the Tibetan crust is segmented by major sub-vertical tectonic structures that separate coherently deformed blocks, and (2) the lower-most 15 to 20 km of the crust beneath southern Tibet is progressively undergoing a phase change which results in a clear

* Corresponding author.

E-mail address: greg@earth.leeds.ac.uk (G.A. Houseman).

¹ Deceased.

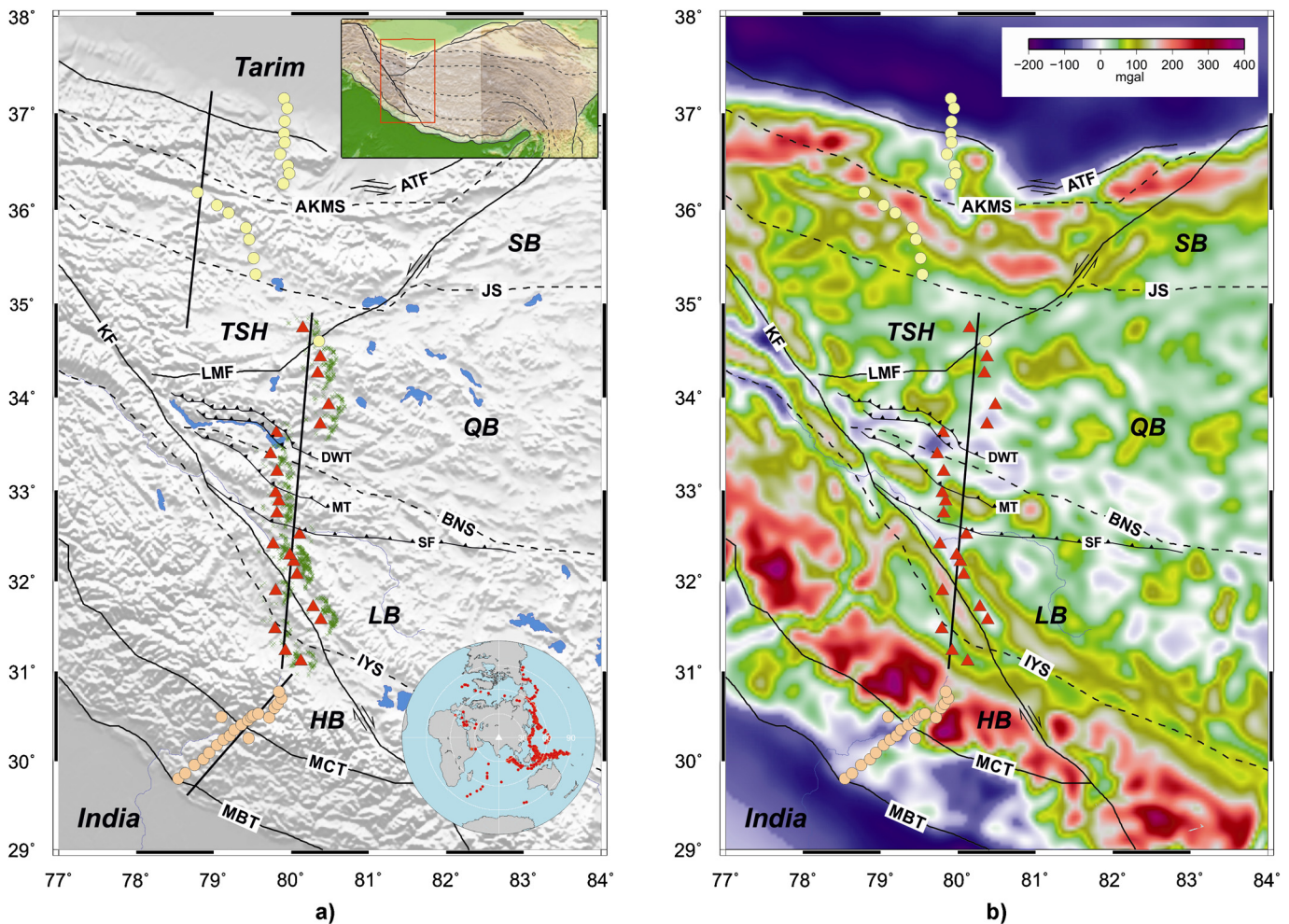


Fig. 1. (a) Map of seismic stations across the western Tibetan Plateau: Red triangles indicate the positions of broadband seismological stations installed for the TW-80 experiment from November 2011 to November 2013. The tan-colored circles show positions of broadband seismological stations used by Caldwell et al. (2013) and Rai et al. (2006) and the yellow circles show stations used in the Sino–French joint project (Wittlinger et al., 2004). The green crosses are the positions of piercing points of PS converted rays at the Moho based on a reference depth of 60 km. Solid lines show projection profiles used by Caldwell et al. (2013), this study, and Wittlinger et al. (2004). Labels denote AKMS: Anyimaqin Kunlun Mustagh Fault; ATF: Altyn Tagh fault; BNS: Bangong–Nujiang suture; DWT: Domar–Wujiang thrust; HB: Himalaya block; IYS: Indus–Yarlung suture; JS: Jinsha suture; KF: Karakoram fault; LB: Lhasa block, LMF: Longmucuo fault; MBT: Main Boundary Thrust of the Himalayan system; MCT: Main Central Thrust; MT: Mandong–Cuobei thrust; QB: Qiangtang block; SB: Songpan block; SF: Shiquanhe fault; TSH: Tianshuihai block. Top inset: Location of study area in Tibetan Plateau. Bottom inset: Distribution map of events with $M_s > 5.0$ and epicentral distances of 30–90° used in this study. (b) Map of TW-80 station locations and major structural features superposed on a map of Free-air gravity anomalies produced using the EGM2008 gridded gravity dataset (Pavlis et al., 2012). The gravity field has been filtered using a Gaussian filter of width 50 km (as defined by GMT routine *grdfilter*).

south to north variation of the seismic properties of the Lhasa block. This lower crustal layer is bounded above by a discontinuity that is similar to the Moho but less strong and 15 or 20 km less deep. The pair of discontinuities that define this layer is similar to that seen beneath the Hi-CLIMB line 5° further east (Nábělek et al., 2009), but here it extends across the entire Lhasa block. Because the segmentation of the Tibetan crust implies that each of the major crustal blocks is deformed coherently, the Indian mantle lithosphere must be similarly deformed unless it detaches from its crust and descends steeply at the latitude of the Indus–Yarlung suture, contrary to the flat subduction mode interpreted, for example, by Nábělek et al. (2009) or Kind and Yuan (2010).

2. Methods

For the TW-80 experiment (Tibet West, longitude 80°E) an array of broadband seismographs was deployed with average station interval of 15–20 km between November 2011 and November 2013 along a 400 km profile at approximately 80°E, between Zarda in southwest Himalaya and Quanshuigou in northwestern Tibet

(for locations see Fig. 1 and Table 1). The TW-80 line crosses the Indus–Yarlung Suture (IYS), the Karakoram fault (KF), the Bangong–Nujiang suture zone (BNS), and other major faults and structures identified on Fig. 1a. During the 24-month observation period from November 2011 to November 2013, 1024 earthquakes with magnitude $M_s > 5.0$, in the distance range 30–90° provided data that were used in the receiver function analysis. Piercing points of the converted rays at the Moho (assumed 60 km depth) are also shown on Fig. 1a, indicating that most events have back-azimuths between about 20° and 180°.

Individual receiver functions (RFs) were estimated by using time-domain iterative deconvolution of vertical and radial seismograms, as described by Ligorria and Ammon (1999). We obtained 3887 receiver functions for the 22 stations along the profile after eliminating those records for which the Moho P_s conversions have a low signal-to-noise (S/N) ratio. A collated section showing the coherence of the individual receiver functions for each station is shown in Fig. 2a.

At each station we processed the available set of receiver functions using the H – κ analysis method of Zhu and Kanamori (2000).

Table 1
Geographic coordinates of the 22 seismic stations used in the TW-80 experiment.

Station	Longitude (deg)	Latitude (deg)	Elevation (m)
St01	80.1227	31.1191	4228
St02	79.9243	31.2302	4192
St03	79.7947	31.4767	3766
St04	80.3865	31.5778	4539
St05	80.2870	31.7193	4457
St06	79.7969	31.8964	4630
St07	80.0762	32.0692	4300
St08	80.0359	32.2144	4267
St09	79.9832	32.2819	4259
St10	79.7669	32.4045	4245
St11	80.1103	32.5137	4300
St12	79.8170	32.7425	4689
St13	79.8402	32.8743	4446
St14	79.8008	32.9715	4391
St15	79.8200	33.1971	4351
St16	79.7299	33.3880	4283
St17	79.8105	33.6200	4281
St18	80.3757	33.7096	4456
St19	80.4851	33.9206	4664
St20	80.3424	34.2581	5221
St21	80.3767	34.4300	5232
St22	80.1536	34.7438	5156

The receiver functions are move-out corrected and stacked for the primary and multiple phases as indicated in Fig. 3 for station ST-07 for a range of plausible H and $\kappa = V_p/V_s$ values. The differing trends in the H - κ space for the primary and its multiples localizes the peak in the stacked function, reducing the trade-off between H and V_p/V_s and thereby enabling these parameters to be jointly

determined. Similar semblance plots were constructed for all stations in order to determine the H and $\kappa (= V_p/V_s)$ values listed in Table 2 and shown in Fig. 4 in relation to the major tectonic features. For many stations, though not all, it is possible to identify two significant discontinuities occurring at different depths (the Moho typically at ~ 9 s, and an earlier arrival of the same polarity ~ 2 s earlier), as is clear in the example of Fig. 3 and the binned stacks of Fig. 2b.

Finally an image section for the TW-80 line (Fig. 5) was constructed by depth migration, using the method described by Yuan et al. (1997), assuming a constant crustal velocity $V_p = 6.3$ km/s and a laterally varying V_p/V_s ratio as determined from the H - κ analysis. In combination with earlier receiver function profiles from the western Himalaya (Caldwell et al., 2013) and the western Songpan-Ganzi and Tarim basin (Wittlinger et al., 2004), these data provide a complete seismic transect across the western Tibetan crust (Fig. 5) for comparison with other sections obtained further east.

The structural interpretation of Fig. 5b is based mainly on the depth-migrated amplitude map given in Fig. 5a, supported by the values of H and V_p/V_s shown in Fig. 4. The H estimates do not exactly overlay the peak values of the migrated receiver function (Fig. 5) because the migration process combines data from different nearby stations using a laterally varying V_p/V_s , whereas the H - κ analysis determines H and V_p/V_s for each station separately. As shown in Fig. 3, decreasing V_p/V_s by 0.05 from 1.74 causes the depth of the seismic discontinuity inferred from the primary converted wave to increase by $\sim 7\%$, other factors being equal. The impact of error in the V_p model is relatively negligible and would affect the entire section in a systematic way, but average V_p for Tibet is well-constrained (Yuan et al., 1997). In Fig. 6 we show also depth-migrated sections for the multiple phases

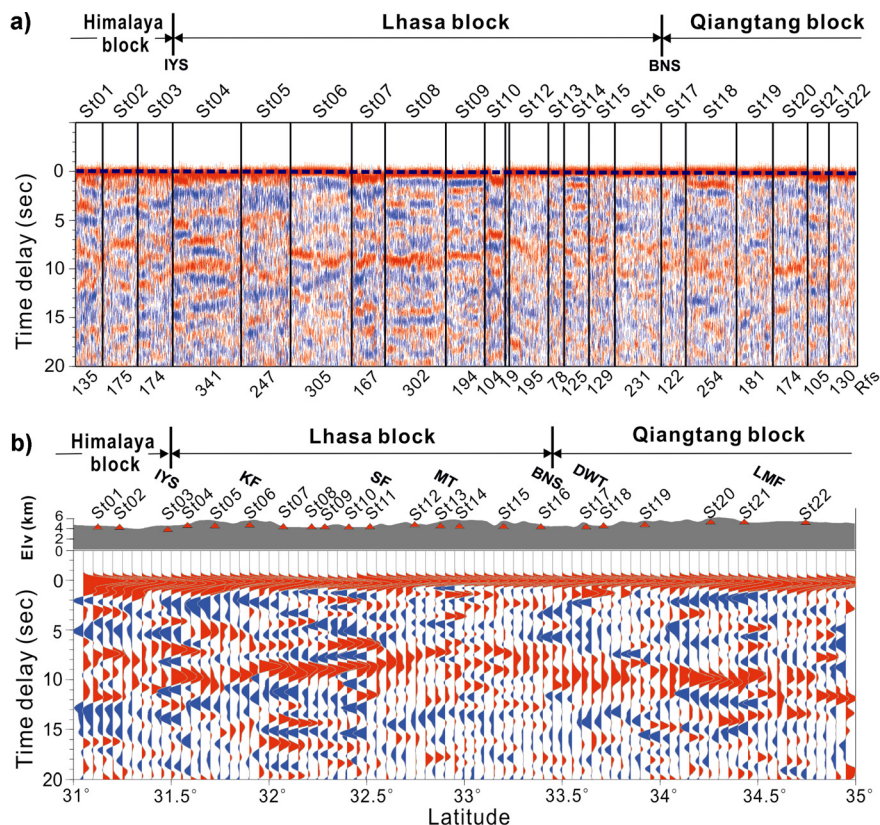


Fig. 2. (a) All raw P_s receiver functions for TW-80, grouped by station number and plotted with constant offset between traces. Red and blue colors show positive and negative amplitudes respectively. Numerical values along the baseline are the number of distinct receiver functions obtained at each station. (b) Stack profile obtained by binning and stacking move-out corrected traces in latitude bins of width 0.1 deg, based on the location of the piercing point at 70 km depth.

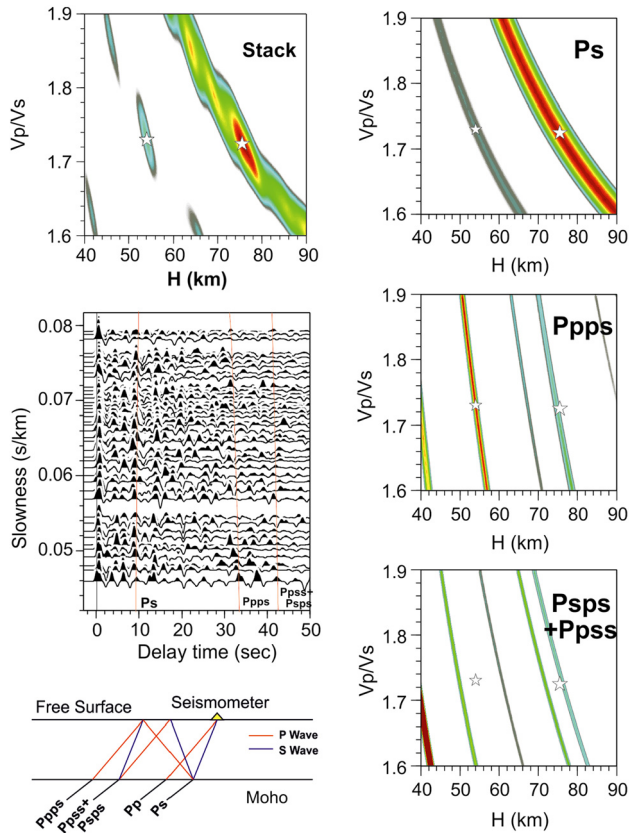


Fig. 3. Analysis of Moho depth and V_p/V_s ratio for station ST-07 obtained using the H - κ stacking method of Zhu and Kanamori (2000), where $\kappa = V_p/V_s$. Individual receiver functions ordered by slowness are shown on the left with vertical lines indicating approximate arrival times of the P_s converted phase and its multiples ($Ppps$ and $Ppsps$). Contours of semblance in the H vs V_p/V_s plane are shown separately for primary signal and each multiple, and for the stack. The intersections of the bands of high semblance for primary and multiples define the preferred values of H and V_p/V_s , as indicated by the white stars; two coherent interfaces are estimated at about 54 km and 75.5 km for ST-07.

$Ppps$ and $Ppsps + Ppsps$ in order to demonstrate consistency of the multiples with the primary converted waves. Although variations in near-surface sediment thickness can produce apparent offsets in structure at depth, we interpret that the relative depth variation of the peak amplitude bands in the lower crust is significant, as are the changes in structure that occur beneath the mapped major structural features. Near the surface the black lines on Fig. 5b are associated with mapped faults and shear zones; in the lower crust these black lines should be interpreted as ductile shear zones rather than seismically active faults.

3. Results

3.1. Crustal structures

The Tibetan crustal structure at 80°E is sub-divided into segments delimited by the major tectonic boundaries. Beneath the southern half of the Lhasa block between 31.3°N and 32.5°N (Fig. 5, from IYS to SF), a large amplitude P_s conversion can be seen with a time delay of ~ 9 s relative to the P phase. For average crustal P velocity of 6.3 km/s and V_p/V_s ratio of 1.74, this arrival originates at a depth of about 70 km. Before this strong converted wave arrives, another less strong P_s conversion from depths of about 55–60 km is observed.

From the Main Central Thrust of the Himalaya the crust rapidly thickens northward to the latitude of the Indus–Yarlung suture zone (IYS). The two converted signals are clearly evident here,

Table 2

For each station, the delay time of the phase P_s determined from each stack, together with best fit H (thickness) and V_p/V_s ratio (κ) as determined from the H - κ analysis using the method of Zhu and Kanamori (2000) (refer to Fig. 4). A second shallower P_s phase was also identified for some stations.

Station	ΔT_{Ps} (s)	H (km)	V_p/V_s	ΔT_{ps} (s)	H (km)	V_p/V_s
St01	8.6541	74.0	1.705	6.0073	54.0	1.670
St02	9.4442	76.5	1.745	7.3369	65.0	1.680
St03	8.7075	71.0	1.740	6.9572	63.0	1.665
St04	9.7421	74.5	1.790	7.0670	56.5	1.755
St05	10.1315	77.0	1.795	7.1145	60.0	1.715
St06	8.5376	72.5	1.710			
St07	9.0752	75.5	1.725	6.5348	54.0	1.730
St08	9.0762	74.5	1.735			
St09	8.6287	77.0	1.675	6.3028	56.0	1.678
St10	9.0094	72.5	1.750	6.4339	57.0	1.680
St11	8.4788	72.0	1.710	6.2899	61.5	1.615
St12	9.0093	71.5	1.655	7.6040	54.5	1.820
St13				7.3684	56.0	1.795
St14	8.3332	67.5	1.745			
St15	8.8548	69.0	1.775	6.8978	57.0	1.730
St16	7.5617	69.5	1.655			
St17	9.7560	71.5	1.825			
St18	9.3128	73.5	1.765			
St19	8.6545	72.0	1.725			
St20	9.9292	75.0	1.800			
St21	9.2388	79.0	1.705			
St22	11.4291	88.5	1.780	9.7898	82.0	1.720

defining a layer between depths of about 50 and 70 km. The smooth northward continuity of this layer is interrupted in two places: First, a minor vertical offset of the Moho ($\lesssim 5$ km) appears to be associated with displacement on either the North dipping IYS or the oblique strike-slip Karakoram Fault (KF) at about 31.8°N. The Karakoram Fault is a major structure on which Miocene age shear zones are well developed (Searle et al., 2011), but on which the magnitude and timing of Quaternary movement is debated (Houlié and Phillips, 2013). A second significant change in the character of the receiver function arrivals and the structure of the crust is associated with the northward dipping Shiquanhe Fault (SF) at about 32.6°N. Whereas these depth offsets are associated with faults observed at the surface, the equivalent structures in the lower crust would be ductile shear zones active during past deformation episodes but not necessarily indicating localization of present-day deformation rates. We note that the radius of the Fresnel zone for wavelengths of ~ 5 km at depths of about 70 km is ~ 20 km and the migration process, in binning arrivals from different receiver locations, introduces further horizontal smoothing. Faults and shear zones of width $\lesssim 20$ km are therefore expected to appear similarly in the migrated images.

Between the Shiquanhe Fault (SF) and the Bangong–Nujiang suture zone at about 33.5°N, the dual converted phases continue to be observed, though both appear shallower and the depth interval between them is reduced to ~ 15 km. Within this northern half of the Lhasa block both the Moho phase and the strong converted wave that precedes it are domed upward, with the shallower phase having a minimum depth of ~ 50 km at about 33°N. North of the BNS in the Qiangtang block the receiver function profile is less well defined, but there is no clear evidence for the shallower phase in this region, and Moho depths are typically 65–70 km between 33.6°N and 34.4°N. The Longmucuo fault (LMF, part of the Jinsha suture) appears to coincide with another major offset in Moho depth; to its north, the strongest conversion occurs at ~ 85 km depth (as found by Wittlinger et al., 2004). Offsets of the Moho may be subtle at IYS/KF, SF, BNS and LMF (Fig. 5), but in each case we see not only differences in Moho depth that may be on the order of 5 to 10 km, but also significant changes in the seismic signature of the crust above the Moho.

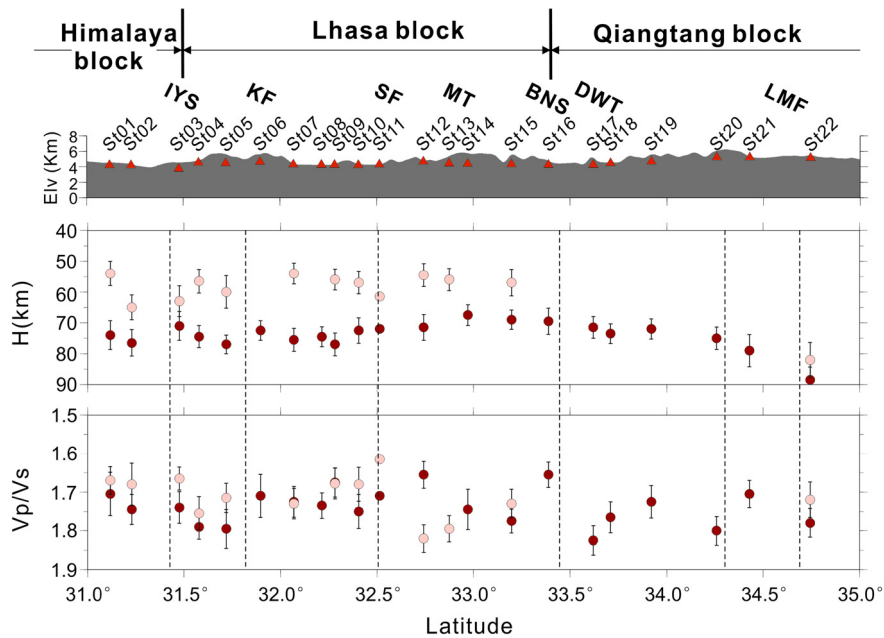


Fig. 4. Profile plots of H and V_p/V_s versus latitude for all 22 stations, shown in relation to the topographic profile and major tectonic features. Where two arrivals are identified, the shallower one is plotted in a light color.

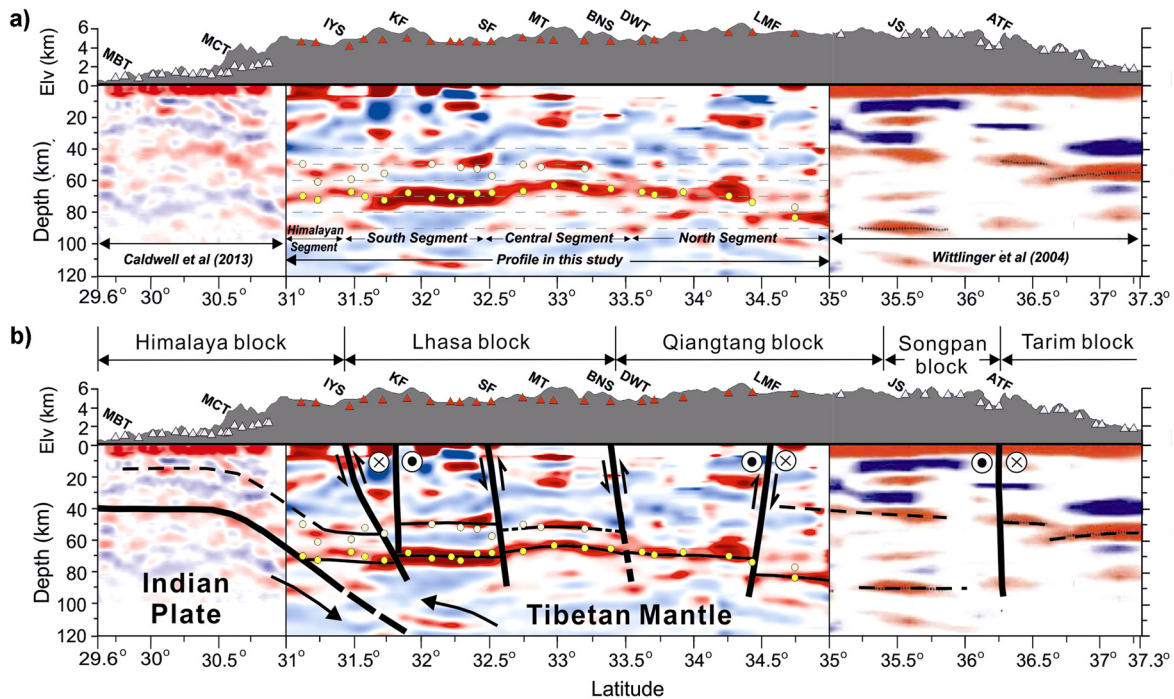


Fig. 5. (a) This 860-km-long transect across western Tibet includes a central panel showing migrated receiver function data from the TW-80 project together with sections previously published by [Caldwell et al. \(2013\)](#) between 29.6°N and 31°N and by [Wittlinger et al. \(2004\)](#) between 35°N and 37.3°N (refer to [Fig. 1a](#) for location of projection lines), all at approximately constant horizontal scale. Colors show migrated receiver function amplitude in the conventional scheme of red for positive amplitude (velocity increasing with depth), blue for negative. Yellow circles show interpreted Moho depths obtained by H - κ analysis for individual stations. Surface topography and projected station locations are shown above the section. Annotation above the topography indicates intersection of major structural features shown on map ([Fig. 1a](#)). (b) Simplified structural interpretation of the western Tibet section superposed on the receiver function section of (a): Sub-vertical black lines represent major faults or shear zones (refer to [Fig. 1a](#) for map location and name of feature); sub-horizontal black lines represent interpreted Moho. The interpreted boundary between Indian-plate mantle lithosphere and Tibetan mantle lithosphere is indicated by the dipping interface that reaches 120 km at 32°N. Arrows show sense of movement associated with major thrusts and strike-slip faults.

3.2. Petrological interpretation

The change in character of both Moho and shallower conversions at the Shiquanhe Fault, (32.6°N) appears to represent a significant difference between northern and southern parts of the Lhasa block. We contrast this structure at 80°E with that from the

Hi-CLIMB experiment at 85°E where the shallower signal above the Moho was only observed in the southern half of the Lhasa block. Following earlier suggestions ([Schulte-Pelkum et al., 2005](#); [Hetényi et al., 2007](#); [Nábělek et al., 2009](#)) that this shallower phase may be explained as the upper bound of a layer of partially eclogitized lower crust, we suggest that south-to-north variations in the

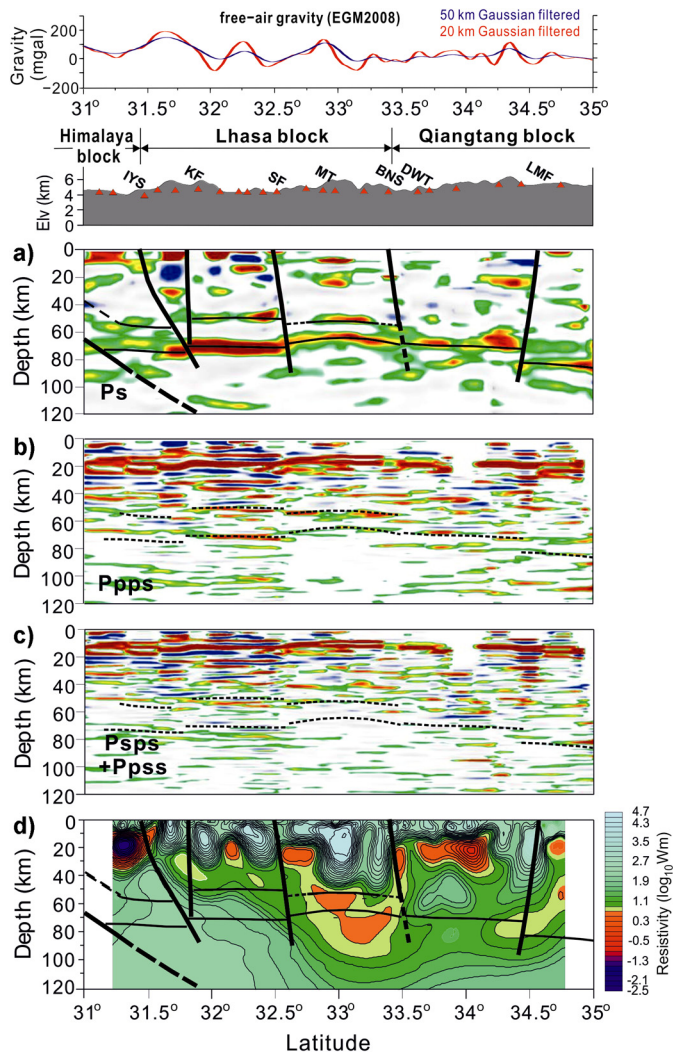


Fig. 6. (a)–(c) Depth-migrated sections for P_s , P_{pps} , and $P_{psps} + P_{pps}$. The velocity model used in migration has a laterally variable V_p/V_s obtained from the H – κ stacking analysis, and a constant P-wave velocity $V_p = 6.3$ km/s. Black lines shown in (a) are the interpreted structures shown on Fig. 5. Dashed sub-horizontal lines shown in (b) and (c) to facilitate comparison of primary and multiple signals are the primary P_s conversions from (a). Plotted above (a), station locations are shown on the topographic profile and smoothed free-air gravity profiles obtained from the EGM2008 gridded gravity data set (Pavlis et al., 2012) are shown for two different spatial smoothing filters. The profile with 50 km filter is for the field shown in Fig. 1b. (d) shows a previously published (Jin et al., 2010) vertical section of the logarithm of apparent electrical resistivity, from a magnetotelluric (MT) profile for the same NS transect across west Tibet. The major features from our structural interpretation of Fig. 5 are superimposed on the resistivity plot at the same scale.

amplitudes and time delays of the two converted signals may be explained by differences in the degree of eclogitization, controlled primarily by the variable presence of water in the crust. As eclogitization progresses, we may expect that the amplitude of the Moho phase decreases relative to that of the shallower phase, and the apparent thickness decreases, since the seismic velocities of eclogite are closer to upper mantle velocities than to crustal velocities. Since eclogitization is a progressive process that occurs according to the availability of hydrous fluids (Hetényi et al., 2007), the systematic change in receiver function signature could be interpreted as lower crustal eclogitization having occurred at an earlier stage in the northern part of the Lhasa block, and having progressed further than in the southern part.

Temperatures and pressures in the Tibetan crust imply that amphibolite-facies metamorphism is likely to be prevalent until transformation to eclogite phase occurs. If that conversion in a

lower-crustal layer is limited by availability of fluids, the properties of that layer may change progressively. Beneath the southern part of the Lhasa block, the high amplitude of the P_s conversion at the Moho could be produced by a layer which is dominantly amphibolite overlying peridotite. Our estimates of V_p/V_s ratios of ~ 1.75 are consistent with those measured for a large suite of amphibolite samples by Ji et al. (2013). Peridotite below the Moho may have originated from Indian plate mantle lithosphere or from asthenosphere that has intruded between the descending mantle lithosphere of the Indian plate and the remnant Indian lower crust. As that lower-crustal layer is progressively metamorphosed to eclogite facies, we expect that the amplitude of the Moho phase decreases and that of the shallower phase increases, because the seismic properties of eclogite are closer to those of peridotite than amphibolite. Comparing the migrated RF section for the southern and northern parts of the Lhasa block (Fig. 5) encourages us in that interpretation.

4. Discussion

4.1. Topography of the Moho

Earlier studies have interpreted Indian-plate mantle lithosphere as intruding horizontally beneath the southern half of the Lhasa block (Nábelek et al., 2009) or even as far north as the Bangong–Nujiang suture zone (Owens and Zandt, 1997). Such models generally envisage an Indian plate that is underthrust beneath Tibetan crust, without undergoing major deformation. If, as interpreted here, the present Tibetan crust has undergone pervasive shortening in vertically coherent blocks, then the underthrusting model is harder to sustain; at least it requires that Indian plate mantle lithosphere has undergone a shortening strain comparable to that of the Tibetan crust. Alternatively, a steeply plunging Indian mantle lithosphere beneath western Tibet, as interpreted by Zhao et al. (2011), separates the problem of how Tibetan crust is shortened and thickened, from what happens to Indian plate mantle lithosphere. The data we present here, unfortunately, do not bear directly on the fate of the Indian-plate mantle lithosphere, but we note that: (1) the preservation of sub-vertical tectonic structures while the crust has been shortened and thickened, and (2) the very strong amplitude of the Moho conversion between 31°N and 32.5°N are both consistent with the idea that Indian-plate mantle lithosphere has separated from crust that has been accreted to the southern edge of Tibet.

Step changes in Moho depth have been reported before: Hirn et al. (1984), using the wide-angle reflection method, found that a step of order 20 km in Moho depth was associated with the IYS at about 88°E ; Vergne et al. (2002) reported steps in Moho depth associated with major tectonic structures from receiver function analyses in the plateau east of 92°E . Other studies (e.g., Kind et al., 2002) do not report evidence for rapid or large variation in Moho depth; wide-angle reflection data from the INDEPTH project (Zhao et al., 2001) suggest that Moho depth only decreases by 2 to 3 km across the Bangong–Nujiang suture at about 89.5°E . Larger offsets in Moho depth are observed across the Altyn Tagh Fault that separates the Tarim Basin from Tibet (Wittlinger et al., 2004), across the boundary between Kunlun Mountains and Qaidam Basin (Zhu and Helmsberger, 1998; Shi et al., 2009) and across the Longmenshan fault that separates the Sichuan Basin from eastern Tibet (Zhang et al., 2009), but the strong lithosphere of the undeforming Tarim, Sichuan and Qaidam blocks is probably necessary to support the stress differences implied by those large and steep changes in crustal thickness.

Deflection of the Moho from horizontal implies significant internal stress caused by the density difference between crust and mantle (even if compensated by internal density variation within

the overlying crust). A northward decrease in free-air gravity anomaly (Pavlis et al., 2012) by about 200 mgal from a local high above the anomalously shallow Moho at about 33.0°N to a relative low at about 33.5°N where the Moho is locally deep beneath the Bangong–Nujiang suture zone (Fig. 1b, Fig. 6) may be influenced by both Moho depth variation and internal density gradients. Although Jin et al. (1994) interpreted the variation of Bouguer gravity across the plateau in terms of folding, such variations in the gravity field could equally be explained by shear zones separating blocks with different internal structure, as depicted in Fig. 5.

Another important consequence of short wavelength variations in Moho depth is that, if the lower crust is strong enough to support stresses associated with such structures, then it is probably too strong to support a lower crustal channel flow of the type described by Beaumont et al. (2001) or Royden et al. (2008). Although a relatively strong Indian-plate mantle lithosphere might also support steps in mantle depth along the TW-80 profile, slow velocities in the uppermost mantle lithosphere of Tibet (Huang et al., 2003; Priestley et al., 2006) and vertically coherent structures within the crust are more simply associated with the idea of a strong lower crust.

4.2. Insights from geodesy, petrology and resistivity

While shear zones imply localized strain it is likely that more strain is accommodated by internal deformation than by relative displacement of the blocks. Although our measurements document strain developed during the continental collision, we note that the northern segment of the Lhasa block (from about 32.5°N to 33.5°N) corresponds to a region of relatively high present-day strain-rate identified by Wang and Wright (2012) using InSAR data; this high strain-rate zone extends west to the Karakoram Fault.

The V_p/V_s ratios inferred from the $H-\kappa$ analysis (Fig. 4) in general are between 1.7 and 1.8. These values are constrained by the requirement that the arrival times of the P_s phase and its multiples are consistent, but the actual uncertainties on these values are probably large enough to prevent a simple interpretation of the observed variations of V_p/V_s along the TW-80 line. Values of V_p/V_s in the range 1.76 to 1.81 are typical for amphibolites or mafic granulites sampled from the North China craton (Kern et al., 1996; Ji et al., 2013) and calculations for the Uralides (Brown, 2007). Estimates of V_p/V_s for eclogites also fall in the same range (Worthington et al., 2013) so this parameter cannot simply be interpreted as a measure of the progress of eclogitization. Some systematic variations in the V_p/V_s ratio are evident however (Fig. 4). Within the southern part of the Lhasa block, V_p/V_s increases northward and is typically greater for the deeper P_s event. There may also be some association of the major vertical structures indicated on Fig. 5 with abrupt changes of the V_p/V_s ratio.

We include finally in Fig. 6d an overlay of our simplified structural interpretation on a depth-section of electrical resistivity from the same transect, obtained from magnetotelluric measurements made along the same line by Jin et al. (2010). The major faults/shear zones are associated with large horizontal gradients of resistivity; these structures may constrain the migration of fluids or melts from one block to another. Low resistivity volumes are found beneath the northern part of the Lhasa block in the lowermost crust and upper mantle, in the same place where we infer from the seismological signature that eclogitization is most advanced. The low resistivities may be an indicator of fluids, which enable the eclogitization reactions to proceed. Low resistivities are also found in the upper crust beneath the Qiangtang block. Comparing the profile of V_p/V_s (Fig. 4) with that of resistivity (Fig. 6d) we note that relatively high values of V_p/V_s coincide with some of the shallow low-resistivity bodies, a correlation which could be caused by partial melt.

5. Conclusions

In summary, these new high-resolution seismic images of the crust across the western Tibetan Plateau provide new insights into the processes that have produced the present day plateau. The major tectonic blocks are bounded by faults or shear zones that cut through the crust to the Moho. A converted phase that precedes the Moho phase beneath the Lhasa block may represent the upper surface of a lower crustal layer that is progressively eclogitized. The eclogitization process requires fluids and is best developed beneath the northern part of the Lhasa block where low resistivities are observed in the lower crust. Beneath the northern Qiangtang block the Moho is up to 90 km deep, the seismic signature of the Moho is more gradational and there is no evidence of the eclogitization or the earlier phase seen at depths of ~55 km beneath the Lhasa block.

Acknowledgements

The project TW-80 was funded by the Strategic Priority Research Program (B) of the Chinese Academy of Sciences (Grant XDB03010700), and Sinoprobe-02-03. Further support was provided by the National Natural Science Foundation of China (Grant nos. 41374062, 41374063 and 41474111). The Seismological Experiment Laboratory, IGGCAS provided instruments for field deployment. The authors also thank G. Hetényi, D. Cornwell, A. Yin, and two anonymous reviewers for constructive comment.

References

- Allegre, C.J., Courtillot, V., Tapponnier, P., Hirn, A., Mattauer, M., Coulon, C., Jaeger, J., Achache, J., Schärer, U., Marcoux, J., et al., 1984. Structure and evolution of the Himalaya–Tibet orogenic belt. *Nature* 307, 17–22.
- Beaumont, C., Jamieson, R., Nguyen, M., Lee, B., 2001. Himalayan tectonics explained by extrusion of a low-viscosity crustal channel coupled to focused surface denudation. *Nature* 414, 738–742.
- Brown, D., 2007. Modal mineralogy and chemical composition of the Uralide lower crust determined from physical properties data. *Tectonophysics* 433, 39–51.
- Caldwell, W.B., Klemperer, S.L., Lawrence, J.F., Rai, S.S., Ashish, 2013. Characterizing the Main Himalayan Thrust in the Garhwal Himalaya, India with receiver function CCP stacking. *Earth Planet. Sci. Lett.* 367, 15–27.
- England, P.C., Houseman, G.A., 1986. Finite strain calculations of continental deformation II: comparison with the India–Asia collision zone. *J. Geophys. Res.* 91, 3664–3676.
- Hetényi, G., Cattin, R., Brunet, F., Bollinger, L., Vergne, J., Nábélek, J.L., Diamant, M., 2007. Density distribution of the India plate beneath the Tibetan Plateau: geophysical and petrological constraints on the kinetics of lower-crustal eclogitization. *Earth Planet. Sci. Lett.* 264, 226–244.
- Hirn, A., Lepine, J., Jobert, G., Spain, M., Wittlinger, G., Xu, Z.X., Gao, E.Y., Wang, X.J., Teng, J.W., Xiong, S.B., Pandey, M.R., Tater, J.M., 1984. Crustal structure and variability of the Himalayan border of Tibet. *Nature* 307, 23–25.
- Houlié, N., Phillips, R.J., 2013. Quaternary rupture behavior of the Karakoram Fault and its relation to the dynamics of the continental lithosphere, NW Himalaya–western Tibet. *Tectonophysics* 599, 1–7.
- Houseman, G., McKenzie, D.P., Molnar, P., 1981. Convective instability of a thickened boundary layer and its relevance for the thermal evolution of continental convergent belts. *J. Geophys. Res.* 86, 6115–6132.
- Huang, Z., Su, W., Peng, Y., Zheng, Y., Li, H., 2003. Rayleigh wave tomography of China and adjacent regions. *J. Geophys. Res.* 108 (B2), 2073. <http://dx.doi.org/10.1029/2001JB001696>.
- Ji, S., Shao, T., Michibayashi, K., Long, C., Wang, Q., Kondo, Y., Zhao, W., Wang, H., Salisbury, M.H., 2013. A new calibration of seismic velocities, anisotropy, fabrics and elastic moduli of amphibole-rich rocks. *J. Geophys. Res.* 118, 4699–4728. <http://dx.doi.org/10.1002/jgrb.50352>.
- Jin, Y., McNutt, M.K., Zhu, Y., 1994. Evidence from gravity and topography data for folding of Tibet. *Nature* 371, 669–674.
- Jin, S., Wei, W.-B., Wang, S., Ye, G.-F., Deng, M., Tan, H.-D., 2010. Discussion of the formation and dynamic signification of the high conductive layer in Tibetan crust. *Chin. J. Geophys.* 53, 2376–2385.
- Kern, H., Gao, S., Liu, Q.-S., 1996. Seismic properties and densities of middle and lower crustal rocks exposed along the North China Geoscience Transect. *Earth Planet. Sci. Lett.* 139, 439–455.
- Kind, R., Yuan, X., 2010. Seismic images of the biggest crash on Earth. *Science* 239, 1479–1480.

- Kind, R., Yuan, X., Saul, J., Nelson, D., Sobolev, S., Mechie, J., Zhao, W., Kosarev, G., Ni, J., Achauer, U., 2002. Seismic images of crust and upper mantle beneath Tibet: evidence for Eurasian plate subduction. *Science* 298, 1219–1221.
- Kosarev, G., Kind, R., Sobolev, S., Yuan, X., Hanka, W., Oreshin, S., 1999. Seismic evidence for a detached Indian lithospheric mantle beneath Tibet. *Science* 283, 1306–1309.
- Kumar, P., Yuan, X., Kind, R., Ni, J., 2006. Imaging the colliding Indian and Asian lithospheric plates beneath Tibet. *J. Geophys. Res.* 111, B06308.
- Li, C., van der Hilst, R.D., Meltzer, A.S., Engdahl, E.R., 2008. Subduction of the Indian lithosphere beneath the Tibetan Plateau and Burma. *Earth Planet. Sci. Lett.* 274, 157–168.
- Liang, X., Sandvol, E., Chen, Y.J., Hearn, T., Ni, J., Klemperer, S., Shen, Y., Tilmann, F., 2012. A complex Tibetan upper mantle: a fragmented Indian slab and no south-verging subduction of Eurasian lithosphere. *Earth Planet. Sci. Lett.* 333–334, 101–111.
- Ligorría, J.P., Ammon, C.J., 1999. Iterative deconvolution and receiver-function estimation. *Bull. Seismol. Soc. Am.* 89, 1395–1400.
- Mechie, J., Kind, R., 2013. A model of the crust and mantle structure down to 700 km depth beneath the Lhasa to Golmud transect across the Tibetan Plateau as derived from seismological data. *Tectonophysics*. <http://dx.doi.org/10.1016/j.tecto.2013.1004.1030>.
- Nábělek, J., Hetényi, G., Vergne, J., Sapkota, S., Kafle, B., Jiang, M., Su, H., Chen, J., Huang, B.S., the Hi-Climb Team, 2009. Underplating in the Himalaya–Tibet collision zone revealed by the Hi-CLIMB experiment. *Science* 325, 1371–1374.
- Ni, J., Barazangi, M., 1984. Seismotectonics of the Himalayan collision zone: geometry of the underthrusting Indian plate beneath the Himalaya. *J. Geophys. Res.* 89, 1147–1163.
- Owens, T.J., Zandt, G., 1997. Implications of crustal property variations for models of Tibetan Plateau Evolution. *Nature* 387, 37–43.
- Pavlis, N.K., Holmes, S.A., Kenyon, S.C., Factor, J.K., 2012. The development and evaluation of the Earth Gravitational Model 2008 (EGM2008). *J. Geophys. Res.* 117 (B4). <http://dx.doi.org/10.1029/2011JB008916>.
- Priestley, K., Debayle, E., McKenzie, D., Pilidou, S., 2006. Upper mantle structure of eastern Asia from multimode surface waveform tomography. *J. Geophys. Res.* 111, B10304.
- Rai, S.S., Priestley, K., Gaur, V.K., Mitra, S., Singh, M.P., Searle, M., 2006. Configuration of the Indian Moho beneath the NW, Himalaya and Ladakh. *Geophys. Res. Lett.* 33 (August), L15308.
- Razi, A.S., Levin, V., Roecker, S.W., Huang, G.D., 2014. Crustal and uppermost mantle structure beneath western Tibet using seismic travel-time tomography. *Geochem. Geophys. Geosyst.* 15, 434–452. <http://dx.doi.org/10.1002/2013GC005143>.
- Ren, Y., Shen, Y., 2008. Finite frequency tomography in southeastern Tibet: evidence for the causal relationship between mantle lithosphere delamination and the north–south trending rifts. *J. Geophys. Res.* 113, B10316.
- Replumaz, A., Tapponnier, P., 2003. Reconstruction of the deformed collision zone between India and Asia by backward motion of lithospheric blocks. *J. Geophys. Res.* 108. <http://dx.doi.org/10.1029/2001JB000661>.
- Replumaz, A., Guillot, S., Villaseñor, A., Negredo, A.M., 2012. Amount of Asian lithospheric mantle subducted during the India/Asia collision. *Gondwana Res.* <http://dx.doi.org/10.1016/j.gr.2012.1007.1019>.
- Rey, P., Teyssier, C., Whitney, D., 2010. Limit of channel flow in orogenic plateaux. *Lithosphere* 2 (5), 328–332.
- Royden, L.H., Burchfiel, B.C., van der Hilst, R.D., 2008. The geological evolution of the Tibetan Plateau. *Science* 321, 1054–1058.
- Schulte-Pelkum, V., Monsalve, G., Sheehan, A., Pandey, M.R., Sapkota, S., Bilham, R., Wu, F., 2005. Imaging the Indian subcontinent beneath the Himalaya. *Nature* 435, 1222–1225.
- Searle, M.P., Elliott, J., Phillips, R., Chung, S.-L., 2011. Crustal–lithospheric structure and continental extrusion of Tibet. *J. Geol. Soc.* 168, 633–672.
- Shi, D., Shen, Y., Zhao, W., Li, A., 2009. Seismic evidence for a Moho offset and south-directed thrust at the easternmost Qaidam–Kunlun boundary in the Northeast Tibetan Plateau. *Earth Planet. Sci. Lett.* 288, 329–334. <http://dx.doi.org/10.1016/j.epsl.2009.09.036>.
- Tapponnier, P., Peltzer, G., Le Dain, A., Armijo, R., Cobbold, P., 1982. Propagating extrusion tectonics in Asia: new insights from simple experiments with plasticine. *Geology* 10, 611–616.
- Tilmann, F., Ni, J., INDEPTH III Seismic Team, 2003. Seismic imaging of the downwelling Indian lithosphere beneath central Tibet. *Science* 300, 1424–1427.
- Vergne, J., Wittlinger, G., Hui, Q., Tapponnier, P., Poupinet, G., Mei, J., Herquel, G., Paul, A., 2002. Seismic evidence for stepwise thickening of the crust across the NE Tibetan Plateau. *Earth Planet. Sci. Lett.* 203, 25–33.
- Wang, H., Wright, T.J., 2012. Satellite geodetic imaging reveals internal deformation of western Tibet. *Geophys. Res. Lett.* 39, L07303. <http://dx.doi.org/10.1029/2012GL051222>.
- Wittlinger, G., Vergne, J., Tapponnier, P., Farra, V., Poupinet, G., Jiang, M., Su, H., Herquel, G., Paul, A., 2004. Teleseismic imaging of subducting lithosphere and Moho offsets beneath western Tibet. *Earth Planet. Sci. Lett.* 221, 117–130.
- Worthington, J.R., Hacker, B.R., Zandt, G., 2013. Distinguishing eclogite from peridotite: EBSD-based calculations of seismic velocities. *Geophys. J. Int.* 193, 489–505. <http://dx.doi.org/10.1093/gji/ggt004>.
- Yin, A., Harrison, T.M., 2000. Geological evolution of the Himalayan–Tibetan orogen. *Annu. Rev. Earth Planet. Sci.* 28, 211–280.
- Yuan, X., Ni, J., Kind, R., Mechie, J., Sandvol, E., 1997. Lithospheric and upper mantle structure of southern Tibet from a seismological passive source experiment. *J. Geophys. Res.* 102, 27491–27500.
- Zhang, Z., Wang, Y., Chen, Y., Houseman, G.A., Tian, X., Wang, E., Teng, J., 2009. Crustal structure across Longmenshan fault belt from passive source seismic profiling. *Geophys. Res. Lett.* 36, L17310.
- Zhao, J., Yuan, X., Liu, H., Kumar, P., Pei, S., Kind, R., Zhang, Z., Teng, J., Ding, L., Gao, X., 2010. The boundary between the Indian and Asian tectonic plates below Tibet. *Proc. Natl. Acad. Sci. USA* 107, 11229–11233.
- Zhao, W., Mechie, J., Brown, L., Guo, J., Haines, S., Hearn, T., Klemperer, S., Ma, Y., Meissner, R., Nelson, K., 2001. Crustal structure of central Tibet as derived from project INDEPTH wide-angle seismic data. *Geophys. J. Int.* 145, 486–498.
- Zhao, W., Kumar, P., Mechie, J., Kind, R., Meissner, R., Wu, Z., Shi, D., Su, H., Xue, G., Karplus, M., Tilmann, F., 2011. Tibetan plate overriding the Asian plate in central and northern Tibet. *Nat. Geosci.* 4, 870–873.
- Zhu, L., Helmberger, D.V., 1998. Moho offset across the northern margin of the Tibetan Plateau. *Science* 281, 1170–1172.
- Zhu, L.P., Kanamori, H., 2000. Moho depth variation in southern California from teleseismic receiver functions. *J. Geophys. Res.* 105, 2969–2980.